

COMPACT MULTIBAND TRANSVERSAL BANDPASS FILTERS WITH MULTIPLE TRANSMISSION ZEROES

X. Zhan^{*}, Z. Tang, H. Liu, Y. Wu, and B. Zhang

School of Electronic Engineering, University of Electronic Science and Technology of China, Chengdu, Sichuan, China

Abstract—Novel compact multiband microstrip transversal bandpass filters (BPF) using short-circuited or open-circuited stub-loaded half-wavelength resonators (SLR) are presented. The dual-band BPF consists of two SLRs and two T-shaped feedlines, and the tri-band BPF can be implemented by a simple reconfiguration of adding one resonator above the original circuit of the dual-band BPF. Multiple transmission zeroes are created to improve the selectivity of the filters. Furthermore, the high degree of design freedom obtained for every passband of dual- or triple-band BPF is achieved by independent resonators and independent signal paths. To verify the proposed concept, two dual-band bandpass filters (filter I and II) and one tri-band bandpass filter (filter III) are designed and fabricated. Both theoretical and measured results are presented, with good agreements.

1. INTRODUCTION

Various wireless standards have emerged into the communication industry, such as global system for mobile communication (GSM), Bluetooth, wireless local-area network (WLAN), and Worldwide Interoperability for Microwave Access (WiMAX). The increasing demand for these applications requires a single wireless system to support multi-standard operations. The multiband filter is the key component in a multiband transceiver. Therefore, the research into filters with multiband operation for RF devices has become popular. In [1, 2], a dual-band filter was implemented by the combination of two individual filters. Extra impedance-matching networks must be utilized to design the input and output structure of the filters. In [3],

Received 5 August 2012, Accepted 29 August 2012, Scheduled 10 September 2012

* Corresponding author: Xiaowu Zhan (ee_wuzi@yahoo.cn).

the concept of the conventional coupling matrix was extended to include designs of dual- and triple-band filters. Besides, the stepped-impedance resonators (SIR) were widely adopted to design multiband filters. A modified half-wavelength SIR with sinuous configuration was constructed to simultaneously excite the dual resonances [4]. The theory of lossless lumped-element equivalent circuit was applied to analyze the tri-band frequency response [5]. In [6], a compact circuit size was obtained by the application of asymmetric SIRs and uniform impedance resonators. In [7], new coupling schemes were proposed to replace the normal counterparts to improve the performance of the filter. SIR filters obtain multiband frequency response by adjusting the ratio of impedance or electronic length, while it is difficult to realize without mutual interference. Several dual-mode resonators of various shapes can result in dual- and tri-band bandpass filters [8–10]. By embedding a pair of slits in the square patch, the dual-band response was generated in [8]. However, the locations of two center frequencies cannot be calculated accurately for the resonator with an asymmetric structure. Although three pairs of degenerate modes were realized in one ring resonator to obtain tri-band frequency response in [9], the filter had a general frequency selectivity and a low degree of design freedom. In [10], since the first and the second passband were achieved by the stub-loaded resonator, the center frequencies of two passbands cannot be controlled independently. In [11], the triple-band filter was implemented by alternately cascaded multiband resonators. However, the number of resonators results in large circuit size and poor insertion loss. A transversal coupling scheme was utilized to design dual-band BPF in [12], but two passbands were formed by different resonators, which is undesirable.

In this letter, we propose novel compact multiband microstrip transversal bandpass filters (BPF) using two different type resonators, namely, the short-circuited stub loaded half-wavelength resonator (SSLR) and the open-circuited stub loaded half-wavelength resonator (OSLR), as shown in Fig. 1. The dual-band BPF is formed by SSLR (Resonator 1) and OSLR (Resonator 2) and a pair of T-shaped feedlines. Meanwhile by adding one OSLR (Resonator 3) to the original circuit of the dual-band BPF, a configuration of the triple-passband BPF is implemented. Several transmission zeroes are realized to improve the filter performance. With every passband achieved by independent resonators and independent signal paths, a high degree of the design freedom is obtained. To verify the proposed concept, two different dual-band BPF (filter I and filter II), and one tri-band BPF (filter III) were designed, simulated, and fabricated.

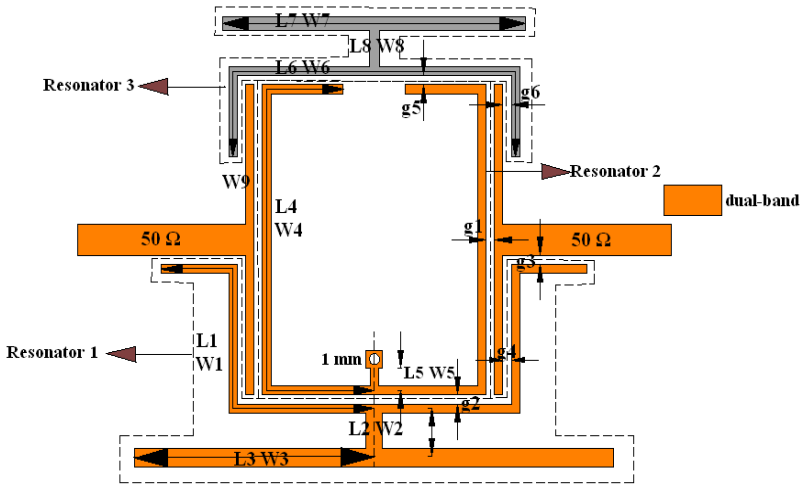


Figure 1. Layouts of the dual- and triple-passband filter.

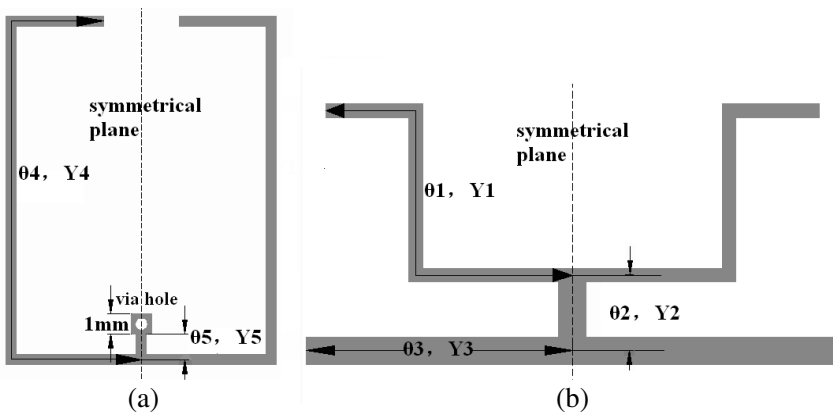


Figure 2. The layout of the resonator: (a) the OSLR, (b) the SSLR.

2. ANALYSIS ON STUB-LOADED RESONATORS

The SSLR (shown in Fig. 2(a)) and the OSLR (shown in Fig. 2(b)) are introduced in the design of the filter. Since both resonators are symmetrical in structure, the odd-even-mode method is implemented. The even-mode circuit is achieved by adding a magnetic wall along the symmetrical plane that can be seen as an open circuit. The odd-mode circuit is achieved by adding an electric wall along the symmetrical

plane that can be seen as a short circuit. $\theta_1, \theta_2, \theta_3, \theta_4$ and θ_5 are electrical lengths of the four sections with lengths L_1, L_2, L_3, L_4 and L_5 , respectively. Y_1, Y_2, Y_3, Y_4 and Y_5 are the characteristic admittances of the widths W_1, W_2, W_3, W_4 and W_5 . Since the length of the short-circuited stub is very short compared with the pad of the via hole, the effect of via pad must be taken into account. C_{via} and L_{via} are the equivalent inductance and capacitance of the via pad.

The input admittance Y_{1even} of the SSLR (Resonator 1) is expressed as:

$$Y_{1even} = -jY_4 \frac{Y_5 (1 - \omega^2 LC - Y_5 \omega L \tan \theta_5) - 2Y_4 \tan \theta_4 (Y_5 \omega L - \tan \theta_5 + \omega^2 LC \tan \theta_5)}{2Y_4 Y_5 \omega L + 2Y_4 \tan \theta_5 (1 - \omega^2 LC) + Y_5 \tan \theta_4 (1 - \omega^2 LC - Y_5 \omega L \tan \theta_4)} \quad (1)$$

$$Y_{1odd} = \frac{Y_4}{j \tan \theta_4} \quad (2)$$

where

$$C = C_{via} = \frac{\varepsilon_0 \varepsilon_r (a^2 - \pi r^2)}{4\pi k h} \quad (3)$$

$$L = L_{via} = \frac{\mu_0}{2\pi} \left[h \ln \left(\frac{h + \sqrt{r^2 + h^2}}{r} \right) + \frac{3}{2} \left(r - \sqrt{r^2 + h^2} \right) \right] \quad (4)$$

where r, a, h and ε_r are the radius of the via hole, width of via pad, thickness of the substrate and relative dielectric constant, respectively.

From the condition $Y_{1even} = 0, Y_{1odd} = 0$, two resonant frequencies of the SSLR in Fig. 2(a) can be extracted as:

$$Y_5 (1 - \omega^2 LC - Y_5 \omega L \tan \theta_5) = 2Y_4 \tan \theta_4 (Y_5 \omega L - \tan \theta_5 + \omega^2 LC \tan \theta_5) \quad (\text{At } f = f_{e1}) \quad (5)$$

$$\theta_4 = \pi/2 \quad (\text{At } f = f_{o1}) \quad (6)$$

According to (5) and (6), it can be found that f_{e1} is lower than f_{o1} .

Similarly, the input admittance Y_{2even} of the OSLR (Resonator 2) is expressed as:

$$Y_{2even} = j \frac{2Y_1^2 Y_2 \tan \theta_1 + Y_1 Y_2^2 \tan \theta_2 + 2Y_1 Y_2 Y_3 \tan \theta_3 - 4Y_1^2 Y_3 \tan \theta_1 \tan \theta_2 \tan \theta_3}{2Y_1 Y_2 - 4Y_1 Y_3 \tan \theta_2 \tan \theta_3 - 2Y_2 Y_3 \tan \theta_1 \tan \theta_3 - Y_2^2 \tan \theta_1 \tan \theta_2} \quad (7)$$

$$Y_{2odd} = \frac{Y_1}{j \tan \theta_1} \quad (8)$$

From the condition $Y_{2even} = 0$ and $Y_{2odd} = 0$, two resonant frequencies of the OSLR in Fig. 2(b) can be extracted as:

$$2Y_1Y_2 \tan \theta_1 + Y_2^2 \tan \theta_2 + 2Y_2Y_3 \tan \theta_3 = 4Y_1Y_3 \tan \theta_1 \tan \theta_2 \tan \theta_3 \quad (\text{At } f = f_{e2}) \quad (9)$$

$$\theta_1 = \pi/2 \quad (\text{At } f = f_{o2}) \quad (10)$$

3. REALIZATION OF THE TRANSMISSION ZEROS

The corresponding coupling schemes for the passbands of two filters are shown in Fig. 3. The signal is coupled to one SSLR and two OSLRs at the same time, providing two independent paths for the signal between the source and load, with no coupling between the source and load. With the notation shown in Fig. 3, the corresponding coupling matrix M can be expressed as

$$M = \begin{bmatrix} 0 & M_{Se} & M_{So} & 0 \\ M_{Se} & M_{ee} & 0 & M_{eL} \\ M_{So} & 0 & M_{oo} & M_{oL} \\ 0 & M_{eL} & M_{oL} & 0 \end{bmatrix} \quad (11)$$

Here, there are some explanations for the coupling matrix. First, since the principle of corresponding coupling schemes shown in Fig. 3 is similar, the Equation (11) is suitable for the analysis on all the passbands of two filters. Second, the relationship $M_{Se} = M_{eL}$ and $M_{So} = -M_{oL}$ holds for the symmetrical configuration.

As shown in Fig. 3(a), a transmission zero can be created near the first passband due to the counteraction between odd-mode signal and even-mode signal of R1 (Resonator 1). Owing to f_{e1} being lower than

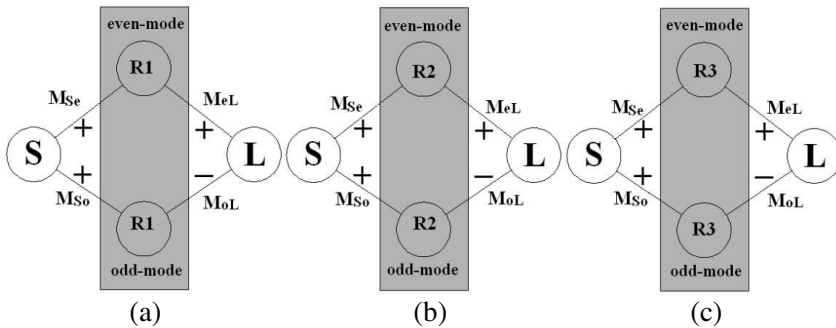


Figure 3. Layouts of the coupling scheme: (a) the first passband of the dual-band filter, (b) the second passband of the dual-band filter, (c) the third passband of the triple-band filter.

f_{o1} , the transmission zero (TZ2) would be in the upper stopband, as explained in [13]. Two additional transmission zeroes (TZ1 and TZ3) are created for the intrinsic characteristic of the dual-mode resonator, i.e., SSLR and OSLR. As explained in [14], the transmission zero Ω is expressed in a low-pass prototype as follows:

$$\Omega = \frac{(M_{oo}M_{Se}^2 - M_{ee}M_{So}^2)}{(M_{So}^2 - M_{Se}^2)} \quad (12)$$

Based on (12), the dual-mode resonator (SSLR or OSLR) exhibits one transmission zero under the relationship $M_{So} \neq M_{Se}$. Besides, the transmission zero can be moved from the upper stopband to the lower stopband, or vice versa, by changing the value of M_{ee} and M_{oo} . The change can be realized by the variation of the loaded stub dimensions. In this paper, since $f_{e1} < f_{o1}$ and $f_{e2} > f_{o2}$, the transmission zero TZ1 and TZ3 would be created at the lower stopband of the first passband and the upper stopband of the second passband, respectively.

4. DESIGN OF THE MULTIBAND BANDPASS FILTERS

As illustrated in [12], the values of coupling coefficient k_1 of the first band and k_2 of the second band can be provided as:

$$k_1 = \left| \frac{f_{o1}^2 - f_{e1}^2}{f_{o1}^2 + f_{e1}^2} \right| \quad (13)$$

$$f_1 = (f_{e1} + f_{o1}) / 2 \quad (14)$$

$$k_2 = \left| \frac{f_{o2}^2 - f_{e2}^2}{f_{o2}^2 + f_{e2}^2} \right| \quad (15)$$

$$f_2 = (f_{e2} + f_{o2}) / 2 \quad (16)$$

where f_1 and f_2 are the central frequencies of the first band and the second band, respectively. Note that two resonators in the dual-band filter can be tuned independently. Thus, appropriate dimensions of two signal paths can be chosen to realize the desired frequency response, according to (5), (6), (9), and (10). When the dimensions of two resonators are fixed, the external factors for the first band and the second band, namely, Q_1 and Q_2 , can be expressed as

$$Q_1 = \frac{2f_1}{\Delta f_{3\text{dB}}^1} = f(g_1, W_9) \quad (17)$$

$$Q_2 = \frac{2f_2}{\Delta f_{3\text{dB}}^2} = f(g_3, g_4, W_9) \quad (18)$$

where $\Delta f_{3\text{dB}}$ is the bandwidth for which the attenuation of S_{21} is 3 dB from its maximum value.

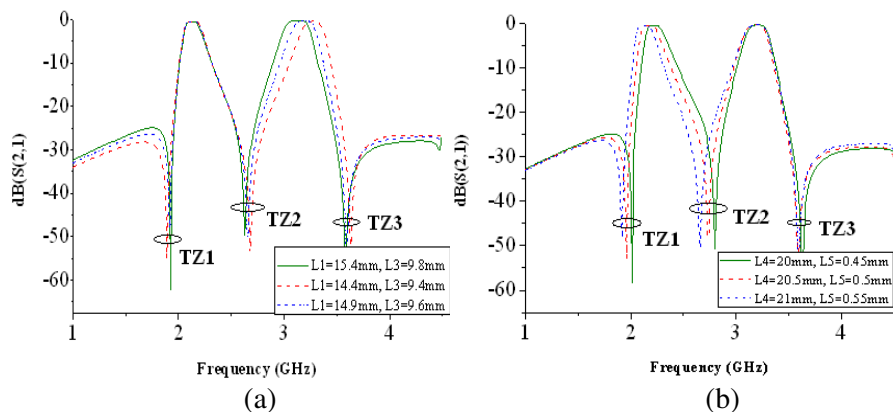


Figure 4. (a) Simulated frequency responses with the variation of L_1 and L_3 , (b) simulated frequency responses with the variation of L_4 and L_5 .

According to (13)–(18), the central frequencies and bandwidth of every passband can be controlled independently, which means the dual-passband filter in this paper has a high degree of design freedom. With the dimensions of the dual-band filter unchanged, the layout of the triple-band filter is implemented by adding Resonator 3 above the dual-band filter, which is shown in Fig. 1. Thus, the triple-band filter possesses the proposed advantage of the dual-band filter.

To embody the high degree of design freedom sufficiently, the simulated results of the filter with the variation of the dimensions of the loaded-stub, i.e., L_1 and L_3 , or L_4 and L_5 , are shown in Figs. 4(a) and (b). It can be noted that one passband center frequency is changed, while the other passband remains essentially unchanged.

4.1. The Simulated and Measured Results of the Proposed Dual-band BPF

In order to fully embody the high degree of design freedom, two dual-band bandpass filters (filter I and filter II) with different passband were simulated and fabricated on Taconic RF-35 substrate with relative dielectric constant of 3.5 and thickness of 0.762 mm. The fabricated dimensions are listed in Table 1. The photograph of two dual-band filters, the simulated and measured results are shown in Fig. 5 and Fig. 6, which show that the design specification is well satisfied. Measured results have a good agreement with the simulation responses. The slight deviation observed can be attributed to fabrication tolerance in the implementation. The measured technology indexes are listed in Table 2.

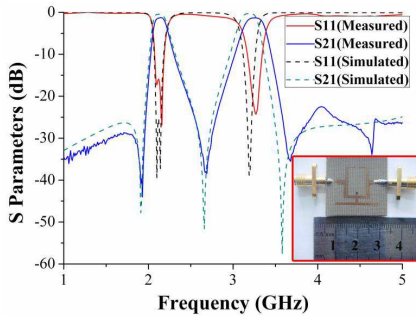


Figure 5. Simulated and measured frequency responses of the filter I.

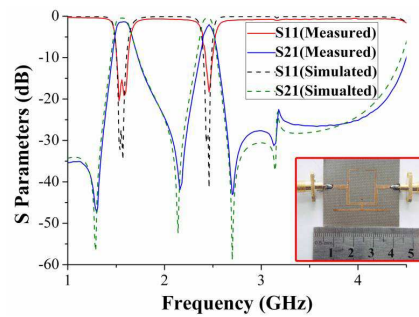


Figure 6. Simulated and measured frequency responses of the filter II.

Table 1. Dimensions of two filters (unit: mm).

	L_1	L_2	L_3	L_4	L_5	W_1	W_2	W_3
Filter I	14.9	2	9.6	21	0.5	0.5	1	1
Filter II	19.9	2	14.25	27.8	1	0.5	1	1
	W_4	W_5	W_9	g_1	g_2	g_3	g_4	
Filter I	0.5	0.5	0.5	0.3	0.2	0.1	0.1	
Filter II	0.5	0.5	0.5	0.2	0.2	0.12	0.12	

Table 2. Measured indexes of the two filters.

Filter I	f_0 /MHz	BW/MHz	Insert loss	Return loss	Isolation	Circuit size
Band 1	2100	170	-1.25 dB	-17.5 dB	-38.5 dB at	323 mm ²
Band 2	3200	270	-1.32 dB	-23.8 dB	2700 MHz	
Filter II	f_0 /MHz	BW/MHz	Insert loss	Return loss	Isolation	Circuit size
Band 1	1570 (GPS)	170	-1.39 dB	-17.1 dB	-41.9 dB at	588 mm ²
Band 2	2450 (WLAN)	110	-2.015 dB	-16.8 dB	2160 MHz	

4.2. The Simulated and Measured Results of the Proposed Triple-band BPF

The tri-passband filter is implemented by adding one open-circuited stub loaded half wave-length resonator (Resonator 3, shown in Fig. 1) above the circuit of the filter II. The tri-passband filter is fabricated on the Taconic RF-35 substrate. The full-wave electromagnetic (EM) simulator is employed for the simulation and optimization of the tri-

band BPF. Fig. 7 shows the photograph of the fabricated BPF, having a dimension of $24\text{ mm} \times 28\text{ mm}$, approximately $0.2\lambda_0 \times 0.23\lambda_0$, where λ_0 is the guide wavelength on the substrate at center frequency of the first passband. The dimensional parameters of the optimal BPF are listed as follows: $L_6 = 24.2\text{ mm}$, $L_7 = 17\text{ mm}$, $L_8 = 2\text{ mm}$, $W_6 = W_8 = 0.5\text{ mm}$, $W_7 = 0.8\text{ mm}$, $g_4 = 0.3\text{ mm}$ and $g_5 = 0.15\text{ mm}$, with other parameters the same as for the dual-band BPF.

Figure 8 illustrates the simulated and measured results, which are in good agreement. As shown in Fig. 8, the proposed filter operates with three passbands located at 1.57, 2.45 and 3.65 GHz, with

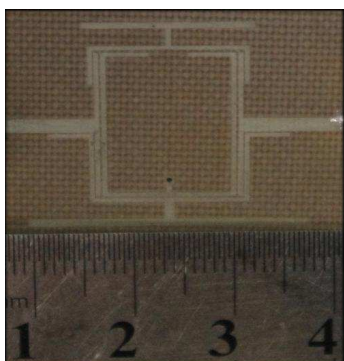


Figure 7. Photograph of the fabricated filter III.

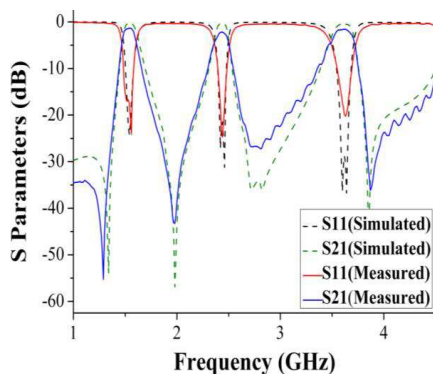


Figure 8. Simulated and measured results of the filter III.

Table 3. Comparison with other proposed triple-passband filters.

Filter	ϵ_r	Center frequencies (GHz)	3 dB FBW (%)	Insertion losses (dB)	Return losses (dB)	Circuit size (mm^2)
[2]	3.38	1.2/2.1/2.54	33/9.5/9.4	-0.5/-1 /-1.3	-14/-17.5 /-18	5016 ($0.43\lambda_0 \times 0.5\lambda_0$)
[9]	10.8	2.35/4.78/7.21	5.3/6.3/8.7	-1.8/-0.9 /-0.7	-21/-23.5 /-21.5	256 ($0.37\lambda_0 \times 0.31\lambda_0$)
[10]	2.55	2.4/3.5/5.5	8/3.7/7.5	-1.4/-1.8 /-1.8	-14/-12 /-12	330 ($0.18\lambda_0 \times 0.26\lambda_0$)
[11]	3.55	2.3/3.7/5.3	3.8/6.8/5	-2.5/-1.9 /-2.9	-18/-18 /-18	1242 ($0.68\lambda_0 \times 0.28\lambda_0$)
This work	3.5	1.57/2.45 /3.65	8.9/6.5/6.4	-1.35/-2.18 /-1.56	Better than -20	672 ($0.2\lambda_0 \times 0.23\lambda_0$)

the measured minimum insertion losses of -1.35 dB, -2.18 dB, and -1.56 dB. The measured 3 dB fractional bandwidths are about 8.9%, 6.5% and 6.4% at the first, second and third passband, respectively. The return losses of three passbands are better than -20 dB. Slight differences in passband frequencies and their corresponding losses between the simulated and measured results are possibly due to unpredictable fabrication error and the insertion loss of SMA connectors. To highlight the advantages of this filter, a comparison with recent works is shown in Table 3.

5. CONCLUSION

In this paper, two novel compact multiband microstrip transversal bandpass filters using two different resonators (SSLR and OSLR) have been presented. The triple-passband filter is implemented by adding one resonator (Resonator 3) above the original circuit of the dual-passband filter. Owing to the intrinsic characteristics of the stub-loaded resonator and the signal counteraction, several transmission zeros are created to improve the filter selectivity. Since the passbands of the two filters are achieved by independent resonators and independent signal paths, a high freedom for design is obtained. Both theoretical and experimental results of the two filters have been provided, with good agreement. Thus, these compact, high degree of design freedom and good performance filter circuits are suitable for the multiband transceivers in the communication system.

REFERENCES

1. Miyake, H., S. Kitazawa, T. Ishizaki, T. Yamada, and Y. Nagatomi, "A miniaturized monolithic dualband filter using ceramic lamination technique for dual mode portable telephones," *IEEE MTT-S Int. Microw. Symp. Dig.*, Vol. 2, 789–792, Jun. 1997.
2. Liu, Y., Y. J. Zhao, Y. G. Zhou, and Z. Y. Niu, "Integrated dual-band BPF and single-band BSF for tri-band filter design," *Journal of Electromagnetic Waves and Applications*, Vol. 25, Nos. 17–18, 2420–2428, 2011.
3. Mokhtaari, M., J. Bornemann, K. Rambabu, and S. Amari, "Coupling-matrix design of dual and triple passband filters," *IEEE Trans. Microw. Theory Tech.*, Vol. 54, No. 11, Nov. 2006.
4. Sun, S. and L. Zhu, "Compact dual-band microstrip bandpass filter without external feed," *IEEE Microw. Wireless Comp. Lett.*, Vol. 15, No. 10, 644–646, 2005.

5. Chen, F. C. and Q. X. Chu, "Design of compact tri-band bandpass filters using assembled resonators," *IEEE Trans. Microw. Theory Tech.*, Vol. 57, 165–171, 2009.
6. Wu, H.-W. and R.-Y. Yang, "Design of a triple-passband microstrip bandpass filter with compact size," *Journal of Electromagnetic Waves and Applications*, Vol. 24, Nos. 17–18, 2333–2341, 2010.
7. Zhang, Y. and M. Sun, "Dual-band microstrip bandpass filter using stepped-impedance resonators with new coupling schemes," *IEEE Trans. Microw. Theory Tech.*, Vol. 54, No. 10, 3779–3785, Oct. 2006.
8. Sung, Y., "Dual-mode dual-band filter with band notch structures," *IEEE Microw. Wireless Compon. Lett.*, Vol. 20, No. 2, 73–75, Feb. 2010.
9. Luo, S., L. Zhu, and S. Sun, "Compact dual-mode triple-band bandpass filters using three pairs of degenerate modes in a ring resonator," *IEEE Trans. Microw. Theory Tech.*, Vol. 59, No. 5, 1222–1229, May 2011.
10. Lin, X.-M., "Design of compact tri-band bandpass filter using $\lambda/4$ and stub-loaded resonators," *Journal of Electromagnetic Waves and Applications*, Vol. 24, Nos. 14–15, 2029–2035, 2010.
11. Chen, C. F., T. Y. Huang, and R. B. Wu, "Design of dual- and triple-passband filters using alternately cascaded multiband resonators," *IEEE Trans. Microw. Theory Tech.*, Vol. 54, 3550–3558, 2006.
12. Zhou, M. Q., X. H. Tang, and F. Xiao, "Compact dual band transversal bandpass filter with multiple transmission zeros and controllable bandwidths," *IEEE Microw. Wireless Compon. Lett.*, Vol. 19, No. 6, Jun. 2009.
13. Rosenberg, U. and S. Amari, "Novel coupling schemes for microwave resonator filters," *IEEE Trans. Microw. Theory Tech.*, Vol. 50, No. 12, 2896–2902, Dec. 2002.
14. Liao, C.-K., P.-L. Chi, and C.-Y. Chang, "Microstrip realization of generalized Chebyshev filters with box-like coupling schemes," *IEEE Trans. Microw. Theory Tech.*, Vol. 55, No. 1, 147–153, 2007.